DALTON
FULL PAPER

Structure, covalence and spin polarisation in tris(acetylacetonato)-ruthenium(III) studied by X-ray and polarised neutron diffraction †

Philip A. Reynolds,*[a] Joe W. Cable,[b] Alexander N. Sobolev[c] and Brian N. Figgis[c]

[a] *Research School of Chemistry, Australian National University, Canberra, ACT 0200, Australia*
[b] *Solid State Division, Oak Ridge National Laboratory, Oak Ridge, Tennessee 37831, USA*
[c] *Department of Chemistry, University of Western Australia, Nedlands, WA 6009, Australia*

A polarised neutron diffraction (PND) experiment on $[Ru(acac)_3]$ at 4.18 K and 5 T along the *b* and *c* axes yielded 28 and 17 flipping ratios respectively. Single-crystal X-ray structure determinations at 293, 92 and 10.5 K, together with powder neutron diffraction experiments, provided auxiliary data allowing magnetic structure factors to be deduced from the PND experiment. The structure is disordered at all temperatures. There are ordered stacks of molecules along *b*, which stacks are arranged in the *ac* plane in two sites of relative displacement 0.4 Å along *b*. The molecular geometries at the sites are similar and approximately D_3 in symmetry, but the magnetisation data indicate C_2 symmetry. The PND data showed significant spin delocalisation by covalence onto the acetylacetonato rings, dominated by spin-polarisation effects, and of C_2 symmetry. However the two data sets differed, with the field along *b* indicating a ^{2}A and that along *c* a ^{2}B dominated state. This cannot be explained in the ligand-field model which fits the magnetic susceptibility data, indicating that vibronic effects must be explicitly considered. Good-quality *ab-initio* local density calculations reproduced the molecular geometry but grossly underestimated the spin correlation between metal and rings.

Studies of bonding in metal complexes have predominantly been based on spectroscopic techniques. Since magnetic properties arise mainly from the valence electrons they are very sensitive to changes in bonding. Spectroscopic techniques which examine magnetic behaviour, especially ESR, are particularly informative. On the other hand, polarised neutron diffraction (PND) probes the spatial rather than energetic aspects of the wavefunction and highlights different features of the bonding. This has proved useful for complexes of the first transition series in defining the balance of factors such as covalence, electron correlation, and the influence of spin–orbit coupling, even in some quite ionic systems.[1] Relative to this transition series, metal ions of the second and third series have more diffuse valence electrons, which consequently do not lie so low in energy. Their energies and radial extents may match better those of the valence orbitals of potential ligand donor atoms and so covalence in the metal–ligand bond may be expected to be higher than for the first series. The higher electric polarisabilities and greater spin–orbit coupling may also produce further differences from the lighter-metal complexes.

In investigations of bonding in heavy transition-metal complexes we have previously used PND to study the $[TcNCl_4]^-$ ion in $[AsPh_4][TcNCl_4]$[2] and the $[Mo(OH_2)_6]^{3+}$ ion in cesium molybdenum alum.[3] We saw high degrees of covalence, particularly in the former case. Here we examine a further example from the second transition series to help establish the degree to which strong covalent effects in the bonding extend to more complex ring systems containing π electrons. The complex is tris(acetylacetonato)ruthenium(III), $[Ru(acac)_3]$, a member of a wide series of $M(acac)_3$ complexes which have been much studied by other physical techniques since they are representative in their properties of many complexes. The crystal structure at room temperature has been determined by X-ray diffraction for the Δ–Λ racemic mixture in two polymorphs[4] and for the pure Δ enantiomer.[5] The magnetic properties of the racemic crystal have been examined by ESR,[6] ^{13}C[7] and ^{1}H NMR spectroscopy,[8] and its single-crystal magnetic susceptibility measured down to 90 K[9] and also recently to 2.5 K along with the magnetisation up to 5 T.[9f] The optical properties of the crystal have been studied in the near IR,[10] and of the molecule in the UV region,[11] and by photoelectron spectroscopy.[12]

In this paper we present the results of a PND study of the racemic compound, with the necessary additional measurements of three improved X-ray diffraction crystal structure determinations at 10.5 and 92 and 293 K, and powder neutron diffraction measurements at 10 and 94 K. Comparison is made with the results of a good-quality *ab-initio* theoretical calculation.

Experimental and Modelling

The complex $[Ru(acac)_3]$ was prepared by a standard method.[13] Single crystals were grown by evaporation of a solution of the compound in benzene. Brown plates up to 70 mg in weight were obtained, with {001} the major faces and {011} and {100} minor faces.

Single-crystal X-ray diffraction

A single crystal of $[Ru(acac)_3]$ was mounted on a Syntex P4 diffractometer of the Crystallography Centre at the University of Western Australia and data measured at 92 K with filtered Mo-Kα ($\lambda = 0.710\,73$ Å) radiation. The diffractometer was equipped with a locally developed nitrogen gas flow low-temperature device. The experimental details and crystal data are summarised in Table 1. Siemens P3/P4-PC software[14] was used for data collection. The data were processed by fitting peak profiles using the program suite PROFIT.[15] Initial models for the structure was taken from ref. 4, and the refinements were carried out with SHELXL 93.[16] Neutral atomic scattering factors were used. The models were refined on data having $F^2 > 2\sigma(F^2)$, minimising using full matrix the quantity $\Sigma[w(F_{obs}^2 - F_{calc}^2)]^2/wF_{obs}^2$, with $w^{-1} = [\sigma^2(F_{obs}^2) + (AP)^2 + BP]$, where $P = (F_{obs}^2 + 2F_{calc}^2)/3$. Corrections for absorption and extinction {secondary, with $F_{calc}^* = kF_{calc}[1 + (0.001F_{calc}^2/\sin 2\theta)]^{\frac{1}{4}}$, where *k* is an extinction coefficient} were carried out. The values of $R = \Sigma||F_{obs}| - |F_{calc}||/\Sigma|F_{obs}|$, goodness of fit $[\Sigma w(F_{obs}^2 - F_{calc}^2)^2/(n-p)]^{\frac{1}{2}}$, where *n* is the number of reflections and *p* the total number of parameters refined, and other coefficients are

† *Non-SI unit employed*: au ≈ 4.36×10^{-18} J.

listed in Table 1. Independent anisotropic displacement parameters were refined for all non-hydrogen atoms, while all hydrogen atoms had isotropic thermal parameters, and those within each methyl group were constrained to be equal. Oxygen and carbon atoms [O(1), O(2), C(1)–C(5)] in the ring which lies nearly perpendicular to the *b* axis apparently have unusually large values of thermal motion along that axis. We call this ring 1, those involving O(3) plus O(4) and O(5) plus O(6) being respectively rings 2 and 3. In the treatment of the present data ring 1 was split into two parts. The individual site occupation factors of the atoms of the split ring were refined. We obtained average site occupation factors of 0.50(2). These were subsequently fixed at a value of 0.5 during further refinement. Identical thermal parameters were assigned to all six half-hydrogen atoms of each Me group in the disordered acetylacetonato group. Significant bond angles and distances are listed in Table 2.

Further data sets at 293 and 10.5 K were collected on a common crystal with a locally assembled X-ray diffractometer and a type 512 Huber goniometer equipped with a Displex DE-202 cryorefrigerator, patterned after the machine of Larsen and coworkers.[17] It uses filtered Mo-Kα X-ray radiation. Details are also collected in Table 1. Locally written diffractometer software was used for data collection and PROFIT and SHELXL 93 for data reduction and structure refinement. Limited searching for superlattice peaks arising from a phase change found none.

The structure at 92 K was used for initial atomic coordinates in the 10.5 K data analysis, but it was quickly found that all atoms not already separated into two sites had extremely anisotropic thermal parameters. Splitting all atoms into two sites produced a stable and improved fit to the data. All non-hydrogen atoms were refined independently with anisotropic displacement parameters. All C–H bond distances were fixed at 0.96 Å, and refined with isotropic displacement parameters constrained equal within each methyl group. The result is two molecules, approximately parallel but separated enough in distance to be resolvable by our data which extend to $(\sin\theta)/\lambda$ 1.06 $Å^{-1}$. The final significant bond angles and distances are given in Table 2. The molecule and the labelling of atoms at 92 K is shown in Fig. 1 and the *ac* unit-cell projection at 10 K in Fig. 2.

The 293 K data were processed similarly, except an absorption correction was not considered necessary given the small effect calculated for the 10.5 K data on the same crystal. The model used at 92 K was found to be appropriate, although the improvement in fit obtained by splitting ring 1 was less marked. Fig. 3 illustrates the evolution of the molecular structure at the three temperatures.

CCDC reference number 186/822.

See http://www.rsc.org/suppdata/dt/1998/559/ for crystallographic files in .cif format.

Powder neutron diffraction

The sample was hydrogenous, so the multiple scattering effects due to the large proton incoherent scattering cross-section were significant. The sample (1 g) was placed in an annular can space, of can diameter 16 mm, but sample thickness only 1 mm so as to reduce multiple scattering. The multidetector medium resolution powder diffractometer at the Australian Nuclear Science and Technology Organisation nuclear reactor HIFAR was used to obtain diffraction patterns at 10.3 and 94.3 K, using a cryorefrigerator. The wavelength used was 1.992(1) Å, and the scattering angular range 2–110°. Each run was of 3 d duration to obtain the good statistics necessary to define the Bragg peaks above the large incoherent background. The data were fitted using scale factor, background, peak profile parameters, unit cell and an overall hydrogen thermal motion parameter as variables, and employing the program GSAS.[18] All other structural parameters, *viz*. atomic unit-cell positions and thermal parameters, were taken from the 10.5 and 92 K X-ray determinations respectively. The hydrogen parameters were modified to give 1.05 Å C–H bond lengths. We obtained at 10 K a fit with R_p 0.0068, wR_p 0.0087 and χ^2 0.93, and at 94 K respectively 0.0077, 0.0097 and 0.98. The overall hydrogen thermal parameters obtained of 330(60) pm^2 at 10 K and 700(100) at 94 K are at about the expected values, and the unit cells agree well with those determined by X-ray diffraction. The fit of the 10.3 K data is shown in Fig. 4.

Ligand-field modelling

For $[Ru(acac)_3]$ the magnetic susceptibility data have been fitted assuming a t_{2g} basis-set description of the $^2T_{2g}$ d^5 ruthenium(III) term with a rhombically distorted trigonal ligand field.[9f] We define in the usual way $t_0 = |0\rangle$, $t_\pm = (2/3)^{\frac{1}{2}}|\mp 2\rangle \pm (1/3)^{\frac{1}{2}}|\pm 1\rangle$. The local axes were chosen so that the trigonal axis is along the weighted mean of the oxygen positions O(1), O(3) and O(5), with the rhombic distortion axis along the mean of O(1) and O(2), ring 1. The minor distortion axis is fixed from the single-crystal magnetisation data.[9f] Saha[9e] showed that the projection of this onto the *ac* plane makes an angle of 56° with *c* and 23° with *a*. As we will show below, one of the acetylacetonato rings behaves differently to the others, and its projection onto *ac* makes angles of 71 and 10° with the axes *c* and *a*. Thus structural and magnetic data both point to this as the minor axis of rhombic distortion. There are four parameters which were used to account for the magnetic data.[9f] They are: ζ, the effective spin–orbit coupling constant; Δ and ε, the trigonal and rhombic ligand-field splittings; and *k*, the Stevens orbital reduction factor.[19] Positive Δ corresponds to a ^2E ground state (split by ε) and a ^2A first excited state, in the absence of spin–orbit coupling.

The temperature dependence, together with the anisotropy, of the magnetic results can be fitted with only one crystal-field solution (Fig. 5). This is the set of parameters CF1: $\Delta = 475$ cm^{-1}, $\varepsilon = -50$ cm^{-1}, $\zeta = 875$ cm^{-1}; $k = 0.7$.[9f] This model gives the first three states at 0, 1195 and 1546 cm^{-1} and moduli of principal values of the *g* tensor of 2.30, 1.29, 1.12. At any given temperature a second crystal field, CF2, can fit the data with parameters *ca*. (depending slightly, but significantly, on temperature) $\Delta = 2900$ cm^{-1}; $\varepsilon = -700$ cm^{-1}, $\zeta = 500$ cm^{-1}, $k = 0.3$, with energies 0, 882 and 3401 cm^{-1} and *g* values varying from 2.33, 1.69, 1.58 at 300 K to 2.33, 1.70, 1.35 at 10 K. The experimental principal *g* values are *ca.* 2.45, 2.16 and 1.45. However the temperature variation of magnetic moments predicted by such a fixed crystal field is about three times less than their observed temperature dependence.

A last point to mention is that the magnetic data show evidence of a small intermolecular antiferromagnetic magnetic coupling as shown by a downturn of all susceptibilities at temperatures approaching 2.5 K.[9f]

DeSimone[6b] has pointed out that for many tris(bidentate ligand) complexes of Fe^{III}, Ru^{III} and Os^{III} there are different acceptable ligand-field model fits to the ESR data. For $[Ru(acac)_3]$ there is better agreement with the CF2 model from the magnetic results than with the CF1 case.

Polarised neutron diffraction

The PND experiment was performed at the HFIR reactor of the Oak Ridge National Laboratory (ORNL), USA, on the diffractometer HB1, with a neutron wavelength of 1.068(1) Å. Neutron polarisation was achieved by use of an iron–silicon monochromator, which gave a polarisation efficiency of 0.901(1). Two *ca*. 50 mg crystals were used, mounted respectively with their *b* and *c* crystal axes parallel to the vertical applied field of 5.00(1) T, at a temperature of 4.18(1) K. Each Bragg reflection was centred manually before counting for the flipping ratio, R_{hkl}, was commenced. The unit cell is consistent with, although less accurate than, the X-ray result, due to the

relaxed resolution of HB1. The parameter R_{hkl} is the ratio of observed diffracted Bragg intensities with neutron spin, respectively, parallel and antiparallel to the applied magnetic field. Flipping ratios were obtained for thirty six *h*0*l* and thirty *hk*0 reflections of high nuclear intensity. After averaging symmetry equivalents, we obtained twenty eight *b*-axis and seventeen *c*-axis unique values of R_{hkl}.

In this centrosymmetric structure if we know the nuclear structure factors then we can calculate values for the *z* component of the magnetic structure factor for these reflections in the basal plane of the diffractometer.[20] For this complex, a structure determined by unpolarised single-crystal neutron diffraction at very low temperatures is not available to give the nuclear structure factors, so we estimated them by use of the 10.5 K X-ray data supported by the powder neutron diffraction results. Recent papers have shown that at these low temperatures a good-quality structure derived from X-ray data can give, within the errors, the same positional and thermal parameters for non-hydrogen atoms as those derived from neutron diffraction data, which fact is generally not true at higher temperatures for a number of reasons amongst which are inadequate treatment of thermal diffuse scattering.[21] The C–H bond lengths were increased to 1.05 Å to correct for the well known apparent shortening observed by X-ray diffraction, and a single isotropic displacement parameter derived from the powder refinement was used. The error introduced by this procedure, which replaces the more usual use of experimental single-crystal neutron data, is consistently less than the uncertainties in the flipping ratios. This is because the major defect, not using individual anisotropic displacement parameters for the hydrogens, becomes serious only at (sin θ)/λ values higher than measured by this PND experiment. The *z* components of the magnetic structure factors for the two orientations are listed in Table 3. The error estimates include the uncertainty in the nuclear structure factors.

Related crystals, isomorphous at room temperature, such as those of $[Al(acac)_3]$ and $[Co(acac)_3]$, develop superlattices at low temperatures.[22] We searched for superlattice nuclear Bragg peaks in the present compound in the *h*0*l* data at 4.18 K in positions suggested by the results for such other crystals and found only count rates below 1 s^{-1}, in the noise, compared to our maximum rate for a peak of 4000 s^{-1}. We conclude that our $[Ru(acac)_3]$ crystal did not show such a phase transition when cooled to 4.18 K.

Spin-density modelling

We used the program ASRED[23] to model the observed magnetic structure factors. Since all the data are in the basal plane, only the *z* component of the magnetisation is observed. Neither this PND experiment nor the magnetic susceptibilities tell us anything about possible canting of magnetic moments relative to the applied magnetic field direction. That would require, for example, the observation of PND reflections which lie out of the basal plane, an experiment that is not possible with the diffractometer HB1.

The number of PND flipping ratios which we measured is limited, and the number of unique atoms in $[Ru(acac)_3]$ is large compared to it, so constraints are necessary in the models used. The first constraint is that both half-molecules are the same and unaffected by the molecular stacking disorder. We then assume a spherical magnetisation density on the ruthenium site composed of orbital and spin components. The data are limited in extent in (sin θ)/λ, so the resolution of anisotropy on any of the atom sites is too poor to be worthwhile. The orbital part of the magnetisation density was modelled in amount and radial extent using the dipole approximation[20] (see also below in polarised neutron diffraction results section) and an ESR *g* tensor.[6a] The radial dependence of the spin part is modified from an ionic Ru^{3+} 4d dependence by a κ expansion, which linearly expands or contracts in (sin θ)/λ the form factor derived from this radial dependence.[24] On the ligands we assume that spin occurs only in the π system on the rings, in $2p_\pi$ orbitals of O and C, with no magnetisation density on the methyl groups. In all cases, we assume *mm* symmetry in each acetylacetonate ring. In each case the fitted data are two-dimensional. This defect has two consequences. First, as already mentioned above, the loss of information related to possible magnetic canting. Secondly, we must assume, and cannot prove, that the magnetisation contributions are atom centred. We are effectively fitting to the Fourier components of a two-dimensional projection of the magnetisation density. In this system this is not serious, because as a molecular insulator, we expect atom-centred contributions to dominate, and also, fortunately, in both crystal orientations the projections of the various ruthenium and ring centres remain well separated; overlap would cause correlation problems between our parameters.

Thus there are three parameters for each acetylacetonate ring, one for each of oxygen and two carbon atoms. Initial refinement of the resultant 11 parameter model gave a satisfactory fit on each data set, with the exception of the total magnetic moments, a point to which we shall return. Examination of the results showed ring 1 differed from 2 and 3, with the latter two similar. We therefore subsequently constrained the ring 2 and 3 populations to be equal giving an eight-parameter model. The results of this model are given in Table 3 for both data sets. The experimental data in Table 3 have been corrected for orbital magnetisation on the Ru using the dipole approximation and normalised, so that all populations refer to spin populations, and total one. This fit gave χ^2 1.31 and a weighted reliability factor, $R_w(F)$, of 0.034 for the *h*0*l* data when the bulk magnetisation was NOT included in the data. A model which required all magnetisation to be located on the ruthenium atom, with none on the rings, raised χ^2 substantially, to 2.74, and $R_w(F)$ to 0.138. For the *hk*0 data the corresponding values for χ^2 and $R_w(F)$ are 1.13 and 0.046 for the covalent model, and 1.60 and 0.106 for the wholly ionic model. Models for covalence requiring three-fold magnetic symmetry, or a pattern of spin density on the ligands suggested by the theoretical calculations [spin on O, C(1) and C(2) in the fixed ratio $1:-0.5:2$], were both some improvement on a purely ionic model, being about midway between the purely ionic model and the best spin model. Inclusion of the bulk magnetisation data[9f] as a constraint on the total magnetisation very severely degraded the fit. We believe that this is because at the experimental temperature and field the paramagnet is only *ca.* 2/3 saturated, and the remaining magnetic disorder significantly depolarises the neutron beams within the crystal. The refinements compared with bulk magnetic data suggest depolarisations of 29 and 68% for the *h*0*l* and *hk*0 data sets respectively. We have observed a comparable degree of depolarisation in cobalt phthalocyanine.[25] In most other systems we have worked at lower temperatures and/or with higher spin quantum numbers, giving a much closer approach to magnetic saturation. In this case the observed magnetic structure factors are thus on a relative scale only.

Ab-initio calculations

We performed calculations using the Amsterdam density functional (ADF) package[26] for $[Ru(acac)_3]$ molecules in both D_3 and C_2 symmetries. These were unconstrained wavefunctions with the Vosko–Wilks–Nusair local density approximation, Becke–Perdew gradient correction, and frozen relativistic atomic cores. We used the atomic bases Dirac Ru 3d, C 1s, O 1s and H in which relativistic core pseudo-potentials are generated from atomic solutions for cores extending to 3d for Ru and 1s for O and C. The remaining valence electrons are fitted using a Slater-type basis of approximately triple-zeta quality. The complete molecular geometry was optimised in D_3 symmetry for the ground ^2E state, excepting only that the three independent C–H

bonds in the methyl group were constrained of equal length, and to make an equal H–C–C angle. The three torsional angles were independently refined. A selection of the geometrical results is given in Table 4. Wavefunctions for the first four excited states (two ^{2}A and two ^{2}B) were also calculated in D_3 symmetry. The Ru–O bond lengths were optimised using the final D_3 structure as starting point, but in C_2 symmetry for the two lowest states ^{2}A and ^{2}B and a third transition state with occupation midway between these (*i.e.* the ^{2}E state in D_3). A full geometry optimisation in this low symmetry was not feasible for us. Mulliken spin populations of those atoms involved in bonding of free acac π orbitals, *i.e.* Ru and the five atoms in each acetylacetonato ring, are given in Table 5 and the lower symmetry C_2 optimisation in Table 6. Spin on the hydrogens and methyl groups is generally small and we neglected it, although it is noticeable in the excited ^{2}B state and first excited ^{2}A state that there is *ca.* 0.015 spin on methyl carbons.

Photoelectron spectroscopy combined with theoretical calculations has shown that, in the valence region, we are concerned with the π interaction of the ruthenium $4d^5$ electrons with the third $acac^-$ π orbital, labelled π_3, each doubly occupied.[12] The HOMO molecular orbitals are $4d_\pi$ ruthenium dominated, while the LUMO is π_4. Our theoretical ADF calculations support this view, and quantify some aspects. However, here we note that the spin populations in Table 5, in which a labelling of states in C_2 symmetry is used, reflect the covalence in the unpaired molecular orbital quite well, and the state energies also reflect the molecular orbital energies. There is some evidence of spin polarisation in the calculation but it is slight. The spin distribution in the unpaired-spin orbital in the ground state is 68% on ruthenium and 32% on the ligand. Spin polarisation increases the ruthenium spin from 68 to 83%, a small, but not negligible effect. In descending from D_3 to C_2 symmetry, A_2 correlates with B, A_1 with A, and E splits into A + B.

We calculate that the octahedral ruthenium(III) ion $^2T_2$ state splits in D_3 to give a ^{2}E ground state, with some 2600 cm^{-1} above it a $^2A_1$ excited state. The spin density in both states is ruthenium dominated, in the $t_\pm$ orbitals occupied in the ^{2}E state and t_0 in the $^2A_1$. Above these three states there are the two further states, ^{2}E and $^2A_1$, which are metal to ligand π_4 charge-transfer states, the ^{2}E 16 500 cm^{-1} above the ground state, $^2A_1$ just above it. Above these at 26 000 cm^{-1} is the ^{2}E state associated with the $4d_\sigma$ spin state. About 8000 cm^{-1} below the $4d_\pi$ HOMO states there is a band of fully occupied π_3 dominated states, which we shall see may be important in spin-polarisation effects.

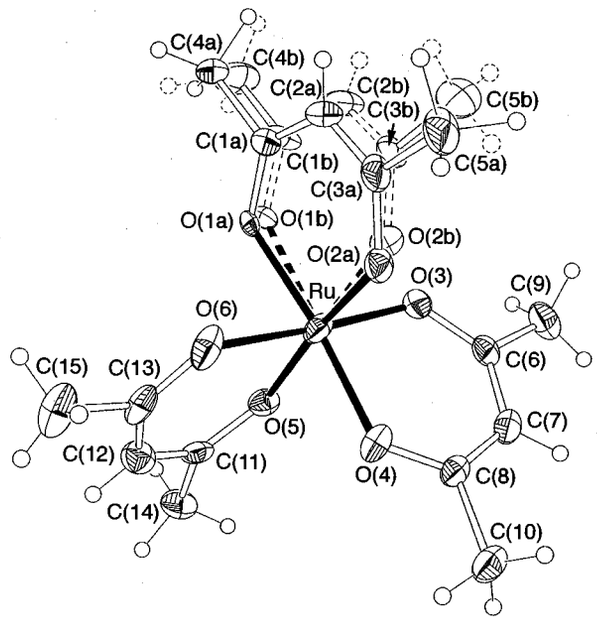

Fig. 1 The [Ru(acac)$_3$] molecule at 92 K; thermal ellipsoids (excluding H) are at the 50% probability level

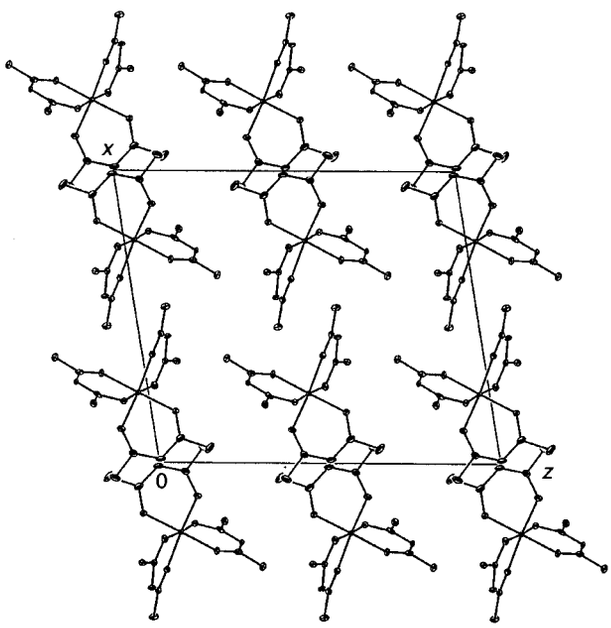

Fig. 2 An *ac* projection of the unit-cell contents at 10 K. For clarity only a single half molecule (molecule A) is shown at each site

Discussion

Crystal disorder and phase behaviour

In this racemic form of the compound the two enantiomers, related by the crystal inversion centre, are defined by the different sign of the twist in their propeller-like molecular conformation. The molecular structure has been fully discussed elsewhere.[4,5] The molecules are of approximately D_3 symmetry, with enantiomeric molecular pairs nested together such that ring 1 of each molecule [O(1)–C(1)–C(2)–C(3)–O(2)] is almost in the *ac* plane and provide the closest intermolecular contacts. This corresponds to an interacting molecular stack along *b*. The ring 1 axis [Ru–C(2)] points roughly along *a* while the molecular approximate three-fold axis points along [−0.12, 1.0, 0.25] or equivalent, *i.e.* rotated about 31° from *b*.

Our 10.5 K data set has sufficient resolution to show that at each molecular site, on average, there are two distinctly resolved molecules, each of half occupancy, which we label A and B. The Bragg scattering shows the average content of the unit cell, and contains no direct information on the contents of individual cells, which must contain either A or B alone. The difference between A and B molecules is mainly associated with motion of ring 1, a flapping with respect to the rest of the molecule, together with a smaller rotation of the whole molecule approximately around an axis close to *c**. Thus the angle between the two Ru–C(2) vectors is 18°, while the angle between the mean of Ru–C(7) and Ru–C(12) is less at 8°. This change is mainly along *b*, with only smaller *ac* components. At 92 K the root mean thermal motion at each site has increased significantly, for example the ruthenium *ac* components increase from *ca.* 8 to 13 pm. Thus the Ru(1A)···Ru(1B) separation at 10.5 K of *ca.* 26 pm can no longer be meaningfully resolved, since it is now just twice the root-mean-square (r.m.s.) thermal motion. This thermal motion is just sufficient to wash out an effectively bimodal probability distribution for Ru and quite sufficient for rings 2 and 3. Thus at 92 K we can model the molecule as single Ru, ring 2 and ring 3 sites with an anisotropic displacement parameter elongated along *b*. However ring 1 still requires two sites adequately to model the data. The 10.5 K C(2A)···C(2B) distance of *ca.* 90 pm would predict this necessity. At 295 K a

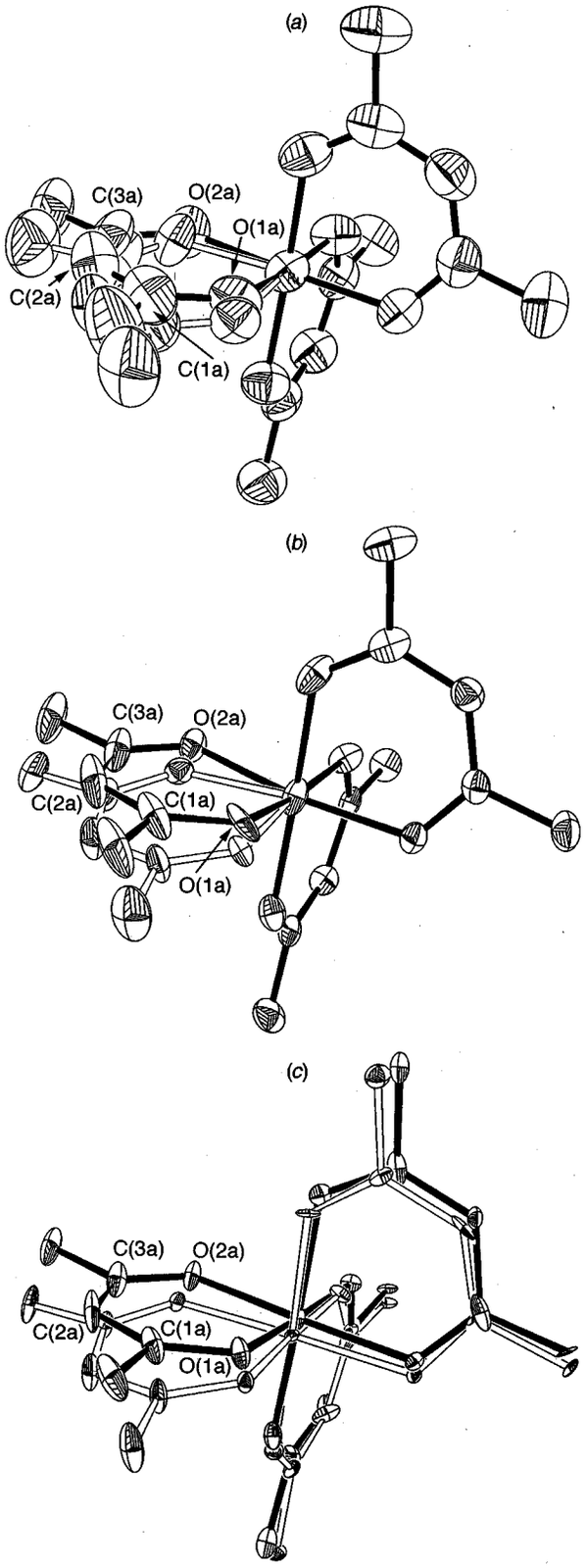

Fig. 3 Projection down a^* of the molecular motion and disorder at (*a*) 295, (*b*) 92 and (*c*) 10 K

predicted root mean square thermal motion of *ca.* 30 pm for the C(2) sites renders these only just resolvable in our data, and not resolvable at all in the less extensive data of Knowles *et al.*[4b] Thus the X-ray data are consistent with a model in which there are two well defined molecular sites whose nature changes little with temperature, but only become resolvable as the temperature, and thus thermal motion, is lowered. This is illustrated in Fig. 3, where the geometry and thermal motion of the molecules projected down a^* are depicted. The converse model of a single site increasingly splitting into two as the temperature is lowered is not supported.

Complete disorder at each site between A and B molecules would imply several close carbon–carbon contacts of 2.7–2.8 Å, all between molecules of the same orientation, both A···A and B···B [*i.e.* C(2B)···C(2B)]. Such short contacts are energetically unacceptable. This shows that the disordered molecules are highly correlated in occupancy. The simplest such correlation is to assume the stacks of molecules along *b* are all alternating in orientation, ABABAB... This makes all intermolecular atom–atom contacts acceptably long. It is possible to arrange such stacks in the *ac* plane in either a long-range disordered or ordered way, and there are many such ordered ways. The compounds $[Al(acac)_3]$ and $[Co(acac)_3]$ have been observed[22] to undergo phase transitions at 140 and 30 K respectively. For $[Al(acac)_3]$ this involves a tripling in the *a* unit-cell length, but no change in space group. Chromium doping in $[Al(acac)_3]$ and EPR spectroscopy shows three sites below, but a single site above, the transition. The three sites below the transition differ in *g*-tensor orientation by 20–30°. These molecular orientational differences and superlattice formation of the other systems in the *ac* plane suggests the disorder in $[Ru(acac)_3]$ is of similar origin.

We observe two orientations but no obvious phase transition, although we searched for the tripled cell explicitly by single-crystal neutron and X-ray diffraction. Given the low $[Co(acac)_3]$ phase-transition temperature, it is possible that this phase of $[Ru(acac)_3]$ does not order at any temperature. To examine this more systematically we performed a powder neutron diffraction experiment. Unlike a conventional single-crystal experiment this surveys all reciprocal space inside a limiting sphere. The difference between A and B sites is so large that long-range ordering in the *ac* plane would dramatically alter the powder neutron diffraction pattern. We observe an excellent fit of experiment and the *ac* disordered structure at both 10.5 and 94 K. Various simulations involving *ac* order produced very poor fits, as expected. This included the simplest situation of simple removal of the centre of symmetry to produce a $P2_1$ symmetry crystal of unchanged cell size. In addition the absences observed in the single-crystal structure also exclude this possibility. A final point is that if we compare the molecule in the present structure with the two independent ones in the pure Δ enantiomer[5] we find that rings 2 and 3 superimpose well, but ring 1 does not. This is further evidence that in the Δ–Λ racemic crystal there is interaction between rings 1 due to crystal-packing effects which causes distortion and disorder.

We conclude that at all temperatures $[Ru(acac)_3]$ consists of molecules whose positions, A or B, alternate along *b*, but that there is no long-range ordering, commensurate or incommensurate, in the *ac* plane. Such a conclusion is testable since it would imply sheets of diffuse intensity in the *ac* plane between the Bragg peaks observable by either single-crystal X-ray or neutron diffraction. The pattern of intensity within the sheets would define local *ac* correlation, which is likely to be present.

Molecular geometry

We discuss first the average values of geometrical parameters of the two molecules. Apart from the ring 1 flap difference between A and B sites, deviations in geometry from D_3 symmetry are significant and well defined. We have collected together data from the 10 K X-ray experiment on the Δ–Λ racemic mixture and from the Δ isomer, averaged into D_3 symmetry, mainly for comparison with theoretical calculations. The room-temperature structure determinations are of lesser accuracy. These experiments illustrate that, while the various independent molecules are approximately of D_3 symmetry, they are significantly distorted. Although for a ^2E ground state we may predict Jahn–

Table 1 Crystal data and structure refinement parameters for [Ru(acac)$_3$]*

T/K	10.5(5)	92(1)	293(2)
Crystal size/mm	0.30 × 0.30 × 0.20	0.23 × 0.23 × 0.18	0.30 × 0.30 × 0.20
D_c/Mg m^{-3}	1.634	1.616	1.545
μ/mm^{-1}	0.993	0.982	0.939
a/Å	13.758(2)	13.819(4)	14.071(4)
b/Å	7.410(1)	7.442(2)	7.534(2)
c/Å	16.095(3)	16.137(5)	16.363(5)
β/°	99.34(1)	99.25(2)	99.05(2)
U/Å^3	1619.1(4)	1638.0(8)	1713.1(8)
θ Range/°	2.56–30.0, 38.75–40.0, 47.50–48.75	2.75–30.0	2.57–25.0
hkl Ranges	−29 to 0, −15 to 15, −29 to 33	−17 to 17, −9 to 9, 0–20	−16 to 16, 0–8, 0–19
Reflections collected	12 357	7433	3141
Independent reflections	6359	3782	3023
R_{int}	0.0170	0.0275	0.0097
Maximum, minimum transmission	0.8370, 0.8062	0.8295, 0.7519	Not applied
Data, parameters	5798, 422	3338, 367	3018, 367
Goodness of fit on F^2	1.163	1.107	1.063
$R(F)$, $wR2$ [$I > 2\sigma(I)$]	0.0280, 0.0640	0.0364, 0.0688	0.0278, 0.0626
(all data)	0.0322, 0.0677	0.0442, 0.0723	0.0357, 0.0705
Weighting coefficients A, B	0.0226, 1.29	0.0181, 2.27	0.0356, 0.47
Extinction coefficient	0.0005(1)	0.0004(1)	0.0042(3)
ρ_{max}, ρ_{min}/e Å^{-3}	0.598, −1.096	0.842, −1.570	0.473, −0.434

* Details in common: $C_{15}H_{21}O_6Ru$, M 398.39; monoclinic, space group $P2_1/c$; $Z = 4$; $F(000)$ 812.

Teller effects, for this weakly π-bonding system, as expected, we observe no static Jahn-Teller distortion. The stereochemistry of the RuO_6 octahedron can be defined by the normalised bite of the bidentate ligand and the angle of twist between the upper [O(1), O(3), O(5)] and lower [O(2), O(4), O(6)] triangular faces.[27] The corresponding parameters of normalised bite and twist angle are 1.45(2) Å and 32(2)°. Other significant conformational parameters of the RuO_6 octahedron, the bite angle O–Ru–O 93(3)° and the bite distance O · · · O 2.91(2) Å, are in good agreement with those for Δ-[Ru(acac)$_3$],[5] 93.0(3)° and 2.906(8) Å. Other geometrical characteristics such as C–O, C–C bonds and corresponding valence angles have normal values (Table 2). The average apparent C–H bond distance is 0.92(6) Å, as expected.

The geometries for the Δ and the Δ–Λ structure, both averaged over 12 independent half-ligand acetylacetonato fragments, agree well with each other. The theoretical ADF calculation results, Table 4, while close, are noticeably different from these averaged values. However we cannot ascribe this difference to a defect in the calculation method, since the spread in the individual observed values, reflected by the maximum and minimum values listed in Table 4, is larger than all these differences. Indeed, given the large ring flap, we should expect this. This is evidence that crystal-packing forces are sufficient significantly to distort the molecule from D_3 symmetry. This is particularly so for the methyl group dihedral rotation angles. This rotation is expected to be of small energy barrier, and is calculated to be so. The observed dihedral angles do not cluster near the global D_3 calculated energy minimum, and are thus dominated by crystal-packing forces.

Bulk magnetism and the ligand field

It has been shown elsewhere[28,29] that ligand-field models can summarise much data, even in very low-symmetry situations, and so provide physical insight. In this case we wish to identify the approximate nature of the ground and low-lying excited states, and subsequently compare with our PND results and theoretical calculations, particularly in the light of the temperature-dependent structural disorder outlined above.

Of necessity we assume both molecular sites have the same properties, although there is some evidence that we are dealing with a weak dimer. Both the structure, with short ring 1–ring 1 interactions distances along b, and the orientation of the rhombic component of the ligand field indicate that intermolecular magnetic interactions can be regarded as an alternating chain along b. The Ru · · · Ru distances alternate between 3.4 and 4.0 Å. These are sufficiently different that the magnetic interaction is probably closer to dimeric than that of a uniform chain. The observability of an ESR signal in the pure crystal, when the magnetic susceptibility around 2.5 K shows some small intermolecular antiferromagnetic interaction, further suggests a localised, perhaps dimer, magnetic interaction. However at higher temperature this weak interaction can be neglected in the discussion of ligand fields.

The magnetic susceptibility down to 90 K shows considerable anisotropy,[9b,c,f] as do the ESR g values.[6] Some ESR data have been interpreted to show that (in D_3 symmetry) either a ^{2}A or ^{2}E ground state can produce suitable principal g values. However, earlier, Saha[9c] showed that the magnetic data unambiguously indicated a ^{2}E ground state for [Ru(acac)$_3$], consistent with the sign of the d-orbital energy splitting deduced for [Ti(acac)$_3$][6] from ESR and for [Os(acac)$_3$] from near IR spectra,[10] that weakly indicated by PES spectra for various acac complexes[12b] and our theoretical ADF calculations. In addition, the ESR g values are very dependent on the crystal environment. Those of Jarrett (2.82, 1.74, 1.28),[6a] from [Ru(acac)$_3$] doped in [Al(acac)$_3$], differ considerably from those (*ca.* 2.45, 2.16, 1.45) of the pure racemic material or various glasses[6b] and values for the pure crystal at particular temperatures are not quoted. It is clear that ^{2}E is the approximate ground-state label in D_3 for [Ru(acac)$_3$], with orbital energies Δ positive, and that the ESR values require a more subtle interpretation.

Given the single-crystal magnetisation data alone, we would choose the ligand-field model CF1 in which all the data are fitted within a single model with a Δ of 475 cm^{-1}. However the g tensor it produces is very different from the observed, with $g_\perp$ 1.20 *versus* the observed 1.51–1.80. The model CF2, with Δ of 2900 cm^{-1} gives $g_\perp$ of 1.52–1.60. In addition this size of the energy Δ agrees much better both with the ADF calculation and the data on [Os(acac)$_3$]. Given the substantial observed temperature dependence of the structure itself, a temperature-dependent crystal field might be expected. An increasing rhombic distortion as the temperature is lowered and as the crystal

Table 2 Bond lengths (Å) and angles (°) for [Ru(acac)$_3$] at different temperatures

	10.5 K		92 K		293 K	
	Molecule A	Molecule B	Molecule A	Molecule B	Molecule A	Molecule B
Ru(1)–O(1)	2.017(2)	2.010(2)	1.965(13)	2.076(12)	1.91(3)	2.13(3)
Ru(1)–O(2)	1.984(2)	2.008(2)	2.003(10)	2.007(11)	1.99(2)	2.01(2)
Ru(1)–O(3)	2.003(2)	1.994(2)	1.999(2)	—	2.005(2)	—
Ru(1)–O(4)	2.005(2)	2.005(2)	2.005(2)	—	2.006(2)	—
Ru(1)–O(5)	1.994(2)	2.031(2)	2.007(2)	—	2.007(2)	—
Ru(1)–O(6)	2.030(2)	2.007(2)	2.020(2)	—	2.019(2)	—
O(1)–C(1)	1.281(4)	1.282(3)	1.32(2)	1.25(2)	1.35(4)	1.21(4)
C(1)–C(2)	1.411(5)	1.397(4)	1.421(14)	1.378(12)	1.45(4)	1.36(4)
C(1)–C(4)	1.516(5)	1.503(4)	1.529(11)	1.501(10)	1.42(4)	1.60(4)
C(2)–C(3)	1.388(5)	1.398(4)	1.362(12)	1.385(10)	1.22(5)	1.49(5)
C(3)–C(5)	1.514(5)	1.503(4)	1.511(13)	1.496(11)	1.48(4)	1.60(4)
O(2)–C(3)	1.277(4)	1.280(3)	1.291(12)	1.282(10)	1.46(4)	1.10(5)
O(3)–C(6)	1.311(4)	1.257(3)	1.279(3)	—	1.271(4)	—
C(6)–C(7)	1.380(4)	1.415(4)	1.394(4)	—	1.390(5)	—
C(6)–C(9)	1.528(4)	1.470(4)	1.503(5)	—	1.498(5)	—
C(7)–C(8)	1.416(4)	1.368(5)	1.399(4)	—	1.385(5)	—
C(8)–C(10)	1.529(4)	1.487(4)	1.508(4)	—	1.501(5)	—
O(4)–C(8)	1.288(3)	1.275(3)	1.280(3)	—	1.273(4)	—
O(5)–C(11)	1.271(4)	1.302(3)	1.280(4)	—	1.276(4)	—
C(11)–C(12)	1.423(5)	1.367(4)	1.396(4)	—	1.382(5)	—
C(11)–C(14)	1.400(4)	1.607(3)	1.495(5)	—	1.505(6)	—
C(12)–C(13)	1.367(4)	1.430(4)	1.392(5)	—	1.393(5)	—
C(13)–C(15)	1.509(5)	1.499(4)	1.509(5)	—	1.505(5)	—
O(6)–C(13)	1.277(3)	1.274(3)	1.266(4)	—	1.260(4)	—
O(1)–Ru(1)–O(2)	93.39(9)	92.64(8)	96.1(5)	88.5(5)	96.9(10)	88.7(9)
O(1)–Ru(1)–O(3)	87.71(9)	87.73(8)	93.7(2)	82.6(2)	91.6(8)	84.9(8)
O(1)–Ru(1)–O(4)	177.42(9)	176.67(8)	172.1(2)	175.8(3)	174.7(8)	176.5(8)
O(1)–Ru(1)–O(5)	90.82(9)	89.47(8)	91.7(5)	89.1(4)	92.3(9)	88.2(9)
O(1)–Ru(1)–O(6)	88.81(9)	89.86(8)	83.4(2)	94.6(2)	85.7(8)	92.4(8)
O(2)–Ru(1)–O(3)	90.70(9)	89.38(8)	95.1(2)	84.8(2)	90.0(7)	88.6(6)
O(2)–Ru(1)–O(4)	87.02(9)	90.54(8)	83.5(2)	93.8(2)	82.3(3)	94.5(3)
O(2)–Ru(1)–O(5)	175.78(9)	176.58(7)	171.0(2)	173.5(2)	170.7(3)	176.1(5)
O(2)–Ru(1)–O(6)	88.60(9)	90.01(8)	84.5(3)	94.3(2)	89.4(7)	90.1(6)
O(3)–Ru(1)–O(4)	94.84(8)	93.27(8)	94.15(8)	—	93.66(9)	—
O(3)–Ru(1)–O(5)	89.29(8)	88.01(8)	88.93(9)	—	88.87(9)	—
O(3)–Ru(1)–O(6)	176.39(8)	177.48(8)	177.00(9)	—	177.09(8)	—
O(4)–Ru(1)–O(5)	88.78(8)	87.39(8)	88.21(8)	—	88.63(9)	—
O(4)–Ru(1)–O(6)	88.65(8)	89.19(8)	88.76(9)	—	89.07(9)	—
O(5)–Ru(1)–O(6)	91.68(8)	92.68(8)	91.92(9)	—	92.20(9)	—
C(1)–O(1)–Ru(1)	123.2(2)	123.2(2)	119.7(10)	127.4(10)	128(2)	120(2)
C(3)–O(2)–Ru(1)	124.6(2)	123.7(2)	122.1(7)	126.7(6)	117(2)	129(2)
O(1)–C(1)–C(2)	126.2(3)	126.4(3)	128.1(9)	123.9(9)	118(3)	132(3)
O(1)–C(1)–C(4)	114.9(3)	113.6(2)	112.6(10)	115.0(9)	119(3)	108(3)
C(2)–C(1)–C(4)	118.9(3)	120.0(3)	119.2(8)	121.1(8)	123(3)	119(3)
C(3)–C(2)–C(1)	126.3(3)	126.1(3)	126.2(7)	127.6(8)	133(3)	122(2)
O(2)–C(3)–C(2)	126.1(3)	126.0(3)	126.4(9)	125.2(8)	127(3)	125(3)
O(2)–C(3)–C(5)	113.6(3)	115.3(2)	113.5(9)	114.9(7)	106(3)	125(4)
C(2)–C(3)–C(5)	120.3(3)	118.7(3)	120.1(8)	119.9(7)	127(4)	109(3)
C(6)–O(3)–Ru(1)	122.1(2)	125.2(2)	123.6(2)	—	123.7(2)	—
C(8)–O(4)–Ru(1)	121.1(2)	124.7(2)	123.0(2)	—	123.2(2)	—
O(3)–C(6)–C(7)	128.8(3)	122.5(3)	125.7(3)	—	125.2(3)	—
O(3)–C(6)–C(9)	109.7(3)	118.3(2)	114.1(3)	—	114.4(3)	—
C(7)–C(6)–C(9)	121.5(3)	119.1(2)	120.1(3)	—	120.4(4)	—
C(6)–C(7)–C(8)	123.0(3)	131.4(3)	127.3(3)	—	128.2(3)	—
O(4)–C(8)–C(7)	130.1(2)	122.8(3)	126.1(2)	—	125.9(3)	—
O(4)–C(8)–C(10)	110.0(2)	119.8(3)	114.8(3)	—	114.4(3)	—
C(7)–C(8)–C(10)	119.9(2)	117.4(2)	119.0(3)	—	119.7(3)	—
C(11)–O(5)–Ru(1)	126.3(2)	121.0(2)	124.2(2)	—	123.7(2)	—
C(13)–O(6)–Ru(1)	121.7(2)	127.1(2)	124.6(2)	—	124.6(2)	—
O(5)–C(11)–C(14)	119.8(3)	109.5(2)	115.0(3)	—	114.3(4)	—
O(5)–C(11)–C(12)	123.9(3)	128.0(2)	125.4(3)	—	125.5(3)	—
C(14)–C(11)–C(12)	116.3(3)	122.3(2)	119.6(3)	—	120.2(4)	—
C(13)–C(12)–C(11)	124.7(3)	128.2(2)	127.0(3)	—	127.9(3)	—
O(6)–C(13)–C(12)	129.8(3)	121.9(2)	125.6(3)	—	124.9(3)	—
O(6)–C(13)–C(15)	112.5(3)	116.6(2)	115.0(3)	—	115.3(4)	—
C(12)–C(13)–C(15)	117.7(3)	121.5(2)	119.5(4)	—	119.9(4)	—

becomes more locally ordered is expected. The stack sequence ABABAB becomes clearer as A and B become more differentiated. It also agrees with the increasing rhombic distortion of the ligand field seen by Andriessen[22] in Cr-doped [Al(acac)$_3$]. We thus prefer the ligand field CF2.

As usual, in [Ru(acac)$_3$], ligand-field models provide a useful method of summarising the ESR and bulk magnetisation data. Their physical significance is often to provide a plausible estimate of the symmetry, of energy spacings in a magnetic field, and of the overall magnetic nature of states thermally access-

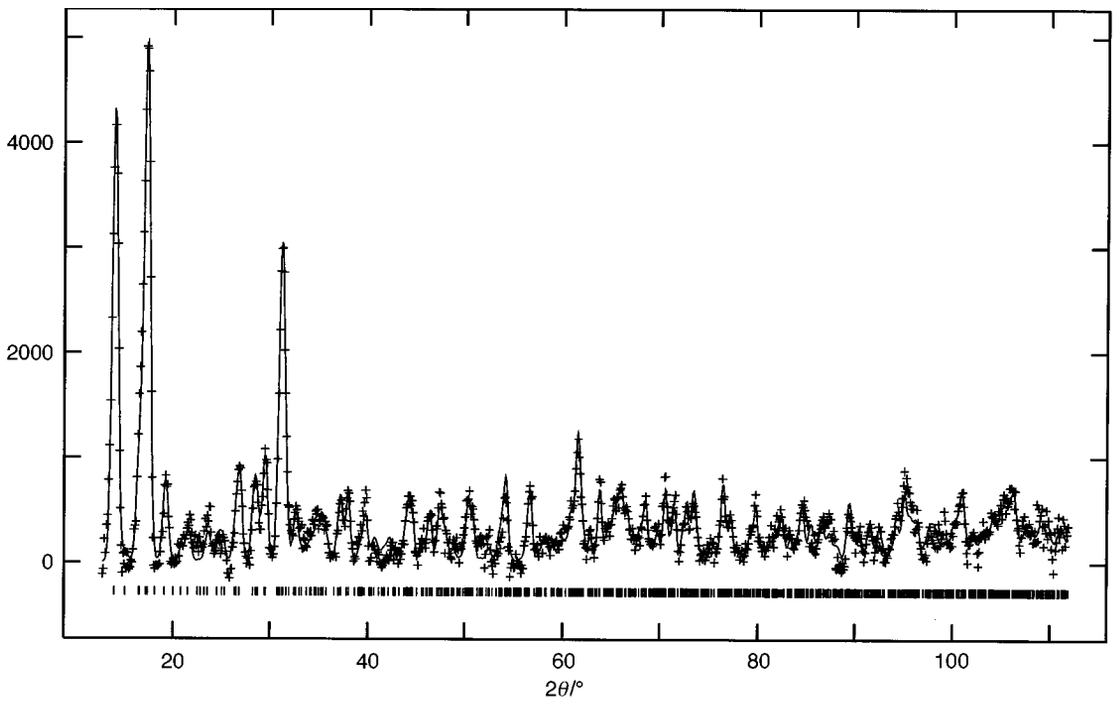

Fig. 4 Neutron diffraction data and fit for powder of [Ru(acac)$_3$] at 10 K

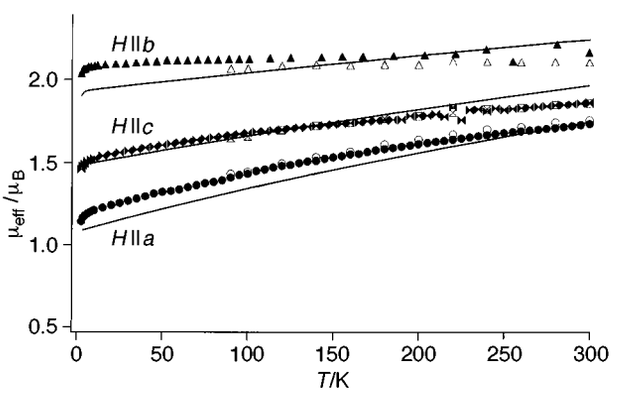

Fig. 5 Single-crystal magnetic susceptibility data for [Ru(acac)$_3$]. The solid lines are the fit of crystal-field model CF1. Solid symbols are the present data, open symbols those of Saha;[9c] $\mu_B \approx 9.27 \times 10^{-24}$ J T^{-1}

ible and with changing populations in the usual 2–300 K experimental temperature range. In [Ru(acac)$_3$] the models indicate that, while the molecular three-fold axis is dominant, there is a substantially broken symmetry defined by ring 1 differing from rings 2 and 3. This is consistent with the fact that ring 1 is different in the structure from rings 2 and 3 in that it is more strongly disordered. This symmetry conclusion is important in that it provides a framework within which more realistic calculations should be made. For example, *ab-initio* calculations in orthorhombic C_2 molecular symmetry may possibly provide a reasonable representation of the situation for the true absence of symmetry, but those like D_3 which assume a three-fold inversion axis certainly will not, at least without some modification. However the PND results below throw considerable doubt on the use of a purely electronic model, such as CF1 or CF2, which does not explicitly include vibronic effects.

Polarised neutron diffraction results

Given the uncertainty in the results of the ligand-field modelling of the available ESR and magnetic properties of [Ru(acac)$_3$], the more detailed investigation of magnetic properties available from PND offers further insight.

In the atom-centred spin populations derived from the experiment, shown in Table 7, as expected, the ruthenium 4d spin density dominates. However, significant moment also appears on the acetylacetonato ligands. There is a tendency for spin populations to be large on the CH carbon, smaller on the corresponding oxygens, and of opposite sign for the intermediate CMe carbon. This is an indication that we are dealing with a combination of spin polarisation and covalence involving the ligand π_3 orbitals, as we describe in the next section.

A complication in the analysis of the PND data is the presence of a contribution to the magnetic scattering from the orbital angular momentum associated with the t_{2g}^5 configuration. Usually, orbital scattering is accounted for using the *dipole approximation*,[20] in which a spherical term proportional to $(g - 2)$ in the second-order scattering factor, $\langle j_2 \rangle$, is added to the $\langle j_0 \rangle$ function which applies for the 'spin-only' case; $\langle j_2 \rangle$ describes a density which is radially more contracted in real space than is that corresponding to $\langle j_0 \rangle$. However, it is known that the dipole approximation is of limited accuracy when the orbital scattering component is large, as it may be here.

A simple experimental measure of the balance of spin polarisation and covalence is the net ruthenium 4d population. Covalence reduces the ruthenium-centred spin population from unity, while spin polarisation increases the ruthenium spin population. As with cobalt phthalocynanine,[25] with $H \| c$, the ruthenium spin population is well above unity at 1.76(10). This indicates that spin-polarisation effects exceed the covalence. For $H \| b$ the population of 0.96(4) indicates that, if covalence is substantial, as our calculation predicts, then covalence and spin polarisation are comparable in size. This comparability has been observed many times by PND,[1] but the effects here are large. However it is also clear that the two data sets differ.

The refinements give different radial extents for the ruthenium spin density from the two data sets, but fixing each at unity does not change the *balance* of spin polarisation and covalence significantly. The dipole approximation used for the orbital moment correction leads to a prediction of a total magnetisation significantly contracted for the $H \| b$ data ($g > 2$) and expanded for the $H \| c$ ($g < 2$), which indeed is what is what is observed. It would appear that the remaining spin moment on the ruthenium, after correction of the orbital moment, still follows the total moment in radial extent. That is, the spin moment is also contracted for the $H \| b$ data and expanded for

Table 3 Observed and calculated magnetic structure factors (μB)

			F_M					F_M	
h	*k*	*l*	obs.	calc.	*h*	*k*	*l*	obs.	calc.
(*a*) *h*0*l* data									
0	0	2	0.519(5)	0.522	2	0	0	−0.720(15)	−0.707
2	0	−4	−0.487(26)	−0.485	2	0	4	−0.293(12)	−0.281
2	0	−6	−0.223(17)	−0.243	0	0	6	0.170(14)	0.170
0	0	8	0.033(9)	0.033	4	0	6	0.000(17)	0.009
8	0	−4	0.209(17)	0.208	8	0	4	0.030(17)	0.009
6	0	−10	−0.020(14)	−0.014	0	0	−12	−0.040(15)	−0.078
10	0	−8	−0.108(40)	−0.008	2	0	2	−0.520(19)	−0.523
6	0	2	−0.252(41)	−0.229	2	0	6	−0.059(23)	−0.084
1	0	−2	−0.270(42)	−0.284	1	0	2	0.277(21)	0.206
3	0	0	−0.185(50)	−0.186	3	0	−2	0.053(25)	0.020
1	0	−4	−0.342(22)	−0.340	1	0	4	0.337(9)	0.339
7	0	0	−0.159(17)	−0.151	7	0	−10	0.017(14)	0.022
11	0	−2	−0.022(28)	−0.011	11	0	2	0.012(27)	0.009
−11	0	10	0.008(26)	−0.029	3	0	2	−0.355(37)	−0.352
(*b*) *hk*0 data									
2	0	0	−0.229(10)	−0.229	1	1	0	−0.217(9)	−0.216
3	0	0	−0.050(8)	−0.049	3	1	0	0.193(17)	0.196
0	2	0	−0.253(19)	−0.259	4	0	0	0.157(14)	0.157
2	2	0	0.185(11)	0.184	4	1	0	0.050(14)	0.055
3	2	0	0.038(14)	0.045	5	0	0	0.030(13)	0.035
5	1	0	−0.095(18)	−0.101	1	3	0	0.149(26)	0.162
7	0	0	0.020(21)	−0.022	6	2	0	0.080(14)	0.065
8	1	0	−0.017(16)	−0.011	4	4	0	0.073(14)	0.044
5	4	0	−0.016(20)	0.013					

Table 4 Experimental and theoretical geometries for the [Ru(acac)$_3$] molecule. Distances are in Å, angles in °

	X-Ray experimental					
	Racemic	Resolved	Minimum	Maximum	ADF theory	Theory minus experimental
Ru–O	2.007	2.003	1.984(2)	2.031(2)	2.056	0.051
O–C	1.281	1.283	1.228(11)	1.311(4)	1.285	0.003
Ru–O–C	123.64	122.5	120.4(9)	127.2(2)	124.26	1.2
C–C (ring)	1.397	1.380	1.341(12)	1.431(4)	1.408	0.020
O–C–C (ring)	125.61	125.9	121.8(2)	130.1(2)	126.31	0.6
C–C (methyl)	1.506	1.506	1.444(19)	1.607(3)	1.513	0.007
O–C–C (methyl)	114.48	114.5	109.7(3)	119.8(3)	114.29	−0.2
C–C (ring)–C	126.62	127.4	123.0(3)	131.4(3)	126.93	−0.1
O–Ru–O (three-fold)	88.80	88.83	87.02(9)	90.82(9)	88.93	0.1
O–Ru–O (bite)	93.07	93.0	90.6(2)	95.0(3)	91.92	−1.1

Table 5 Mulliken spin populations (electrons × 10^4) for the ground and first four excited doublet states of [Ru(acac)$_3$] calculated using the ADF method (small hydrogen populations omitted)

State	Approximate nature	*E*/au	Ru	O(1)	C(1)	C(2)	O(5)	C(11)	C(12)	O(6)	C(13)
A	$t_{\pm}$ Ru 4d	−9.514	8343	45	73	−15	279	−163	564	290	−192
B	$t_{\pm}$ Ru 4d	−9.514	8307	363	−253	753	135	−34	191	126	2
A	t_0 Ru 4d	−9.502	9325	−6	19	−6	−6	19	−6	−6	−6
A	π_3 Ligand	−9.440	425	98	6	9	932	−170	3270	763	33
B	π_3 Ligand	−9.439	−32	1275	−103	3259	787	17	237	872	−27

the $H\|c$ data. One explanation would be that the spin polarisation, which is not constrained to be 4d-like in radial extent on the ruthenium site, is strongly influenced by the orbital magnetisation. This then causes the total change in radial extent to be enhanced over that predicted solely by use of the dipole approximation.

However, as noted earlier, these data depart very significantly from three-fold symmetry in ligand atom populations. Moreover, if we attempt simultaneous refinement of both the *h*0*l* and *hk*0 data sets in the same C_2 symmetry covalent model we obtain a very poor fit, no better than for a purely ionic model with no spin on the ligand rings at all. Thus the spin on the ligands is very different in pattern for the magnetic field applied along the *b* and along the *c* axis directions. An *empirical* rationalisation is that the molecular ^{2}E symmetry is broken. For the $H\|c$ results the ring 1 population is greater than that of rings 2, 3 by 0.06 spins, while for the $H\|b$ results it is less than them by 0.30 spins. Table 5 shows that the calculated covalent spin transfer into ring 1 is greater than into rings 2, 3 for the ^{2}B state, while the opposite is true for the ^{2}A state. This pattern is also what we qualitatively expect from simple molecular orbital arguments. Thus, if the populations from spin polarisation are relatively uniform over the rings, the data with $H\|c$ arise from a ^{2}B-like state while those with $H\|c$ arise from ^{2}A.

We can quantify this pattern for each of the data sets. For $H\|c$ we require spin populations due to covalence in the unpaired MO of *ca.* +0.6 on Ru, +0.2 on ring 1, and +0.1 on rings 2, 3, about the same as is calculated theoretically in the ADF calculations. To obtain the observed total spin pattern we then require a spin polarisation of the other six bonded electrons to give the ruthenium spin population of +1.2 with each ring receiving a population of −0.4 spins. This approximates the observed total spin by giving Ru +1.8, ring 1 −0.2 and rings 2, 3 −0.3 spins each. We can compare this to the observed values of +1.8(1), −0.21(6) and −0.27(6) spins respectively. Turning to the $H\|b$ data, we require the ^{2}A contribution from covalence to the $H\|b$ data to be Ru +0.6, ring 1 0.0, rings 2, 3 +0.2 spins. This maintains the overall three-fold symmetry required by the sum of the ^{2}A and ^{2}B covalent contributions. If this is modified by spin polarisation giving a contribution to the ruthenium spin population of +0.3 and −0.1 on each ring we obtain calculated net spin populations of Ru +0.9, ring 1 −0.1, rings 2, 3 +0.1. Compared to the observed populations Ru +0.96(4), ring 1 −0.19(2), rings 2, 3 +0.11(4) spins there is satisfactory agreement.

While the spin populations quoted above cannot be regarded as more than semiquantitative illustrations, we deduce from the PND experiment that (1) the $H\|b$ data involve a ^{2}A state and the $H\|c$ data a ^{2}B dominated state, (2) covalence is substantial, delocalising *ca.* 40% of the unpaired spin and (3) spin-polarisation effects are at least comparable to those of covalence, and are substantially greater for the $H\|c$ than for the $H\|b$ data.

Comparison of the PND results and *ab-initio* theory

The results of the ADF *ab-initio* calculation can be summarised qualitatively as follows. In the isolated acetylacetonato ligand the lowest two ligand π orbitals are roughly carbonyl bonding in nature, the next higher in energy is π_3 with majority C–H carbon $2p_\pi$, and the next two higher are carbonyl antibonding in nature. The trigonal distortion is large enough, and the overlap small enough, that the doubly occupied ruthenium $4dt_0$ and the doubly occupied A_1 symmetry acetylacetonato π_3 combination do not mix significantly. We thus accommodate four up- and three down-spin electrons, three originating from ruthenium and four from the ligands, in the four E symmetry molecular orbitals formed from the ruthenium 4d $t_\pm$ orbitals and the two acetylacetonate π_3 orbitals of E symmetry. We expect the unpaired spin to reside mainly in the ruthenium 4d $t_\pm$ orbitals, but to be delocalised to some extent onto the ligand ring. The unpaired electron spin in the ruthenium 4d $t_\pm$ orbitals will cause spin polarisation of the three pairs of spin-paired electrons, causing a positive (or spin-up) build up of spin on the ruthenium site, and negative (or spin-down) on the ligand. Covalence and spin polarisation thus produce opposing effects. Given that we are dealing with six spin-polarisable electrons of the same symmetry as that of the spin-unpaired electron we cannot ignore spin polarisation. However examination of the molecular orbital coefficients in the theoretical calculation shows surprisingly little spin polarisation of spin-paired orbitals in any of the states.

If we now compare the experimental populations with the ADF calculation we see that the spin delocalised by covalence in the unpaired orbital is reproduced quite well; 32% is calculated and 40% observed. On the other hand the spin polarisation is highly underestimated. The ADF calculation increases the ruthenium-centred spin resulting from spin polarisation by only 15% of the total spin, whereas we observe 36 and 110% respectively in the two orientations of the magnetic field. It appears that the ADF molecular calculation seriously underestimates the long-range spin correlations in the crystal. In the previous case of $[TcNCl_4]^-$ [2b] that was not so. There a single unpaired spin can this time spin-polarise eight chlorine in-plane π electrons. In cobalt phthalocyamine we also observed by PND that spin polarisation outweighed the covalence effects,[25] as was also true on the manganese sites in $[Mn_{12}O_{12}(CD_3CO_2)_{16}(D_2O)_4]\cdot 2CD_3CO_2D\cdot 4D_2O$ observed by unpolarised powder diffraction methods.[30] Again, in the $[CoCl_4]^{2-}$ ion in Cs_3CoCl_5 in order to fit the PND data the theoretical wavefunction of Cassam-Chenai *et al.*[31] required eight determinants, with the ground state-dominated determinant having a coefficient of only 0.44, indicative of strong correlation effects.

The density functional calculation relies on uniform electron gas calculations to estimate correlation effects. For long-range π correlations as specific as those between the ruthenium 4d $t_\pm$ and the acetylacetonate π_3 orbital this may not be adequate, although it appears to be so for the shorter-range correlations possible in a Tc–Cl bond. The longer M–L bonds calculated relative to experiment, 0.05 Å for Ru–O and 0.035 Å for Tc–Cl, may also reflect the extra binding obtained by a proper treatment of correlation. An alternative or perhaps additional factor is that both shorter M–L bonds and extra spin correlation arise from crystal-packing forces. Such forces will tend to compress bonds, particularly the weak M–L bonds. In addition they will raise the energy of the ligand π_3 orbitals, producing better energy matching and thus covalence with the ruthenium 4d $t_\pm$ orbitals. Additional covalence will produce more spin polarisation, which may overwhelm the loss of ruthenium spin density by covalence. The difference between the $H\|b$ and $H\|c$ data in amount of spin polarisation suggests that crystal packing plays some role, and there is obvious relationship to the apparent change in symmetry of the ground state from ^{2}A to ^{2}B.

Table 6 Calculated optimised geometry and energy in C_2 symmetry using the ADF method

		Ru–O/Å	
State	*E*/au	Ring 1	Rings 2, 3
^{2}A	−9.5156	2.0571	2.0552
^{2}B	−9.5155	2.0555	2.0560
^{2}E	−9.5145	2.0558	2.0558

The ground states and ligand-field theory

The ligand fields, whether CF1 or CF2, resulting from the fit to the magnetic data have a clear prediction that the ground state is an isolated molecular doublet in which A and B electronic character are about equally present. Application of magnetic fields does not substantially change this within the ligand-field model. Thus the drastic changes in spin populations observed

Table 7 Mulliken spin populations (electrons × 10^3) for the ground and first excited doublet states of $[Ru(acac)_3]$ calculated using the ADF method, compared with experimental values obtained from the PND results

	Ru	O(1)	C(1)	C(2)	O(5)	C(11)	C(12)	κ
A	834	5	7	−2	28	−16	56	—
B	831	36	−25	75	13	−3	19	—
$H\|b$	962(35)	7(16)	−56(15)	−87(16)	57(20)	−38(29)	73(44)	0.81(4)
$H\|c$	1759(109)	−96(48)	−1(61)	−17(87)	−62(36)	34(55)	−217(73)	1.30(14)

in the PND as the applied magnetic field is changed clearly contradict the ligand-field prediction.

The crystal disorder and intermolecular effects, while a complicating factor, do not alter this conclusion. The resulting slight splittings and/or dispersion within a ground-state band will not cause a magnetic field to select A- or B-like components from the mixed state.

An explanation in vibronic terms is probably required. It is possible that we may have, by coupling of vibrational and electronic states, a situation in which there are several vibronic states, some A and some B in electronic character, close in energy but of differing magnetic behaviour. This provides a plausible qualitative explanation of the PND observations: the intermolecular interactions perturb the isolated D_3 symmetry molecule such that a magnetic field can select vibronic states of differing spatial electronic symmetry. We would thus have a subtle blend of inter- and intra-molecular effects to consider in any quantitative theory.

Acknowledgements

We thank the Australian Research Council, the Australian Department of Industry, Trade and Tourism, and the Australian Institute of Nuclear Science and Energy for financial support to B. N. F. and P. A. R. We acknowledge the contributions to the growth of crystals made by Dr. L. M. Engelhardt (University of Western Australia). We also thank Dr. S. J. Kennedy of the Australian Nuclear Science and Technology Organisation for collaboration in the collection of the powder neutron diffraction data. A part of the present research was carried out at the Oak Ridge National Laboratory under Contract No. DEAC05-84OR21400 with Martin Marietta Energy Systems Inc.

References

1 B. N. Figgis, J. B. Forsyth, E. S. Kucharski, P. A. Reynolds and F. Tasset, *Proc. R. Soc. London*, *Ser. A*, 1990, **428**, 113; P. J. Brown, B. N. Figgis and P. A. Reynolds, *J. Phys.: Condens. Matter*, 1990, **2**, 5309; C. D. Delfs, B. N. Figgis, J. B. Forsyth, E. S. Kucharski, P. A. Reynolds and M. Vrtis, *Proc. R. Soc. London*, *Ser. A*, 1992, **436**, 417.

2 (*a*) B. N. Figgis, P. A. Reynolds and J. W. Cable, *J. Chem. Phys.*, 1993, **98**, 7743; (*b*) P. A. Reynolds, B. N. Figgis, J. B. Forsyth and F. Tasset, *J. Chem. Soc.*, *Dalton Trans.*, 1997, 1447.

3 S. P. Best, B. N. Figgis, J. B. Forsyth, P. A. Reynolds and P. L. W. Tregenna-Piggot, *Inorg. Chem.*, 1995, **34**, 4605.

4 (*a*) G. K.-J. Chao, R. L. Sime and R. J. Sime, *Acta Crystallogr.*, *Sect. B*, 1973, **29**, 2845; (*b*) T. S. Knowles, M. E. Howells, B. J. Howlin, G. W. Smith and C. A. Amodio, *Polyhedron*, 1994, **13**, 2197; (*c*) T. S. Knowles, B. J. Howlin, J. R. Jones, D. C. Povey and C. A. Amodio, *Polyhedron*, 1993, **12**, 2921.

5 H. Matsuzawa, Y. Ohashi, Y. Kaizu and H. Kobayashi, *Inorg. Chem.*, 1988, **27**, 2981.

6 (*a*) H. S. Jarrett, *J. Chem. Phys.*, 1957, **27**, 1298; (*b*) R. E. DeSimone, *J. Am. Chem. Soc.*, 1973, **95**, 6238.

7 D. M. Doddrell and A. K. Gregson, *Chem. Phys. Lett.*, 1974, **29**, 512; D. Waysbort, *J. Phys. Chem.*, 1978, **82**, 907; D. M. Doddrell, D. T. Pegg, M. R. Bendall and A. K. Gregson, *Aust. J. Chem.*, 1977, **30**, 1635; D. M. Doddrell, D. T. Pegg, M. R. Bendall, H. P. W. Gottlieb, A. K. Gregson and M. Anker, *Chem. Phys. Lett.*, 1976, **39**, 65.

8 D. R. Eaton, *J. Am. Chem. Soc.*, 1965, **87**, 3097; D. M. Doddrell, D. T. Pegg, M. R. Bendall, P. C. Healy and A. K. Gregson, *J. Am. Chem. Soc.*, 1977, **99**, 1281.

9 (*a*) B. N. Figgis, J. Lewis, F. E. Mabbs and G. A. Webb, *J. Chem. Soc. A*, 1966, 422; (*b*) A. K. Gregson and S. Mitra, *Chem. Phys. Lett.*, 1969, **3**, 392; (*c*) M. Saha, *Indian J. Phys.*, 1969, **43**, 646; (*d*) R. Grobelny, B. Jezowska-Trzebiatowska and W. Wojciechiwski, *J. Inorg. Nucl. Chem.*, 1966, **28**, 2715; (*e*) A. Earnshaw, B. N. Figgis and J. Lewis, *J. Chem. Soc. A*, 1966, 1656; (*f*) B. N. Figgis, P. A. Reynolds, B. Moubaraki and K. S. Murray, *Aust. J. Chem.*, in the press.

10 R. Dingle, *J. Mol. Spectrosc.*, 1965, **18**, 276.

11 H. Kobayashi, H. Matsuzawa, Y. Kaizu and A. Ikeda, *Inorg. Chem.*, 1987, **26**, 4318.

12 (*a*) S. Evans, A. Hamnett, A. E. Orchard and D. R. Lloyd, *Discuss. Faraday Soc.*, 1972, **54**, 227; (*b*) A. Yu. Ustinov, M. E. Akopyan and G. M. Svistunov, *Russ. J. Phys. Chem.*, 1993, **67**, 1067.

13 A. Johnson and G. W. Everett, *J. Am. Chem. Soc.*, 1972, **94**, 1419.

14 Siemens P3/P4-PC software, revision 4.27, 1991.

15 V. A. Streltsov and V. E. Zavodnik, *Sov. Phys. Crystallogr.*, 1989, **36**, 824.

16 G. M. Sheldrick, SHELXL 93, Program for Crystal Structure Refinement, University of Göttingen, 1993.

17 K. Henriksen, F. K. Larsen and S. E. Rasmussen, *J. Appl. Crystallogr.*, 1986, **19**, 390; F. K. Larsen, *Acta Crystallogr.*, *Sect. B*, 1995, **51**, 468.

18 A. C. Larson and R. B. von Dreele, LANSCE, MS-H805, Los Alamos National Laboratory, Los Alamos, NM, 1991.

19 K. W. H. Stevens, *Proc. R. Soc. London*, *Ser. A*, 1953, **219**, 542.

20 W. Marshall and S. W. Lovesey, *Theory of thermal neutron scattering*, Oxford University Press, Oxford, 1971.

21 B. B. Iversen, F. K. Larsen, B. N. Figgis, P. A. Reynolds and A. J. Schultz, *Acta Crystallogr.*, *Sect. B*, 1996, **52**, 923; B. B. Iversen, F. K. Larsen, P. A. Reynolds and B. N. Figgis, *Acta Chem. Scand.*, 1994, **48**, 800.

22 W. T. M. Andriessen, *J. Phys. Chem. Solids*, 1976, **37**, 189.

23 B. N. Figgis, P. A. Reynolds and G. A. Williams, *J. Chem. Soc.*, *Dalton Trans.*, 1980, 2339.

24 P. Coppens, T. N. Guru-Row, P. Leung, E. D. Stevens, P. Becker and Y. P. Yang, *Acta Crystallogr.*, *Sect. A*, 1979, **35**, 63.

25 P. A. Reynolds and B. N. Figgis, *Inorg. Chem.*, 1991, **30**, 2294; G. A. Williams, B. N. Figgis and R. Mason, *J. Chem. Soc.*, *Dalton Trans.*, 1981, 734.

26 C. Fonseca Guerra, in *Methods and Techniques in Computational Chemistry*, eds. E. Clementi and G. Corongiu, STEF, Cagliari, 1995; G. te Velde and E. J. Baerends, *J. Comput. Phys.*, 1992, **99**, 84; E. J. Baerends, D. E. Ellis and P. Ros, *Chem. Phys.*, 1973, **2**, 41.

27 D. L. Kepert, *Inorganic Stereochemistry*, Springer, Berlin, 1982.

28 M. Gerloch, *Magnetism and Ligand Field Analysis*, Cambridge University Press, Cambridge, 1983.

29 A. B. Blake, C. D. Delfs, L. M. Engelhardt, B. N. Figgis, P. A. Reynolds, A. H. White, B. Moubaraki and K. S. Murray, *J. Chem. Soc.*, *Dalton Trans.*, 1993, 1417.

30 P. A. Reynolds, E. P. Gilbert and B. N. Figgis, *Inorg. Chem.*, 1996, **35**, 545.

31 G. S. Chandler, B. N. Figgis, R. A. Phillips, P. A. Reynolds, R. Mason and G. A. Williams, *Proc. R. Soc. London*, *Ser. A*, 1982, **384**, 31; P. Cassam-Chenai, S. K. Wolff, G. S. Chandler and B. N. Figgis, *Int. J. Quantum. Chem.*, 1996, **60**, 667.

Received 15*th September* 1997; *Paper* 7/06681C